Simulating option price dynamics with exponential quantum speedup

Javier Gonzalez-Conde,[1,*] Ángel Rodríguez-Rozas,[2] Enrique Solano,[3,4,5] and Mikel Sanz[1,3,6,†]

[1]*Department of Physical Chemistry, University of the Basque Country UPV/EHU, Apartado 644, 48080 Bilbao, Spain*
[2]*Risk Division, Banco Santander, Avenida de Cantabria S/N, 28660 Boadilla del Monte, Madrid, Spain*
[3]*IKERBASQUE, Basque Foundation for Science, Plaza Euskadi 5, 48009, Bilbao, Spain*
[4]*International Center of Quantum Artificial Intelligence for Science and Technology (QuArtist) and Department of Physics, Shanghai University, 200444 Shanghai, China*
[5]*Kipu Quantum, Kurwenalstrasse 1, 80804 Munich, Germany*
[6]*Basque Center for Applied Mathematics (BCAM), Mazarredo Zumarkalea, 14, 48009 Bilbao, Spain*

(Dated: February 3, 2022)

Pricing financial derivatives, in particular European-style options at different time-maturities and strikes, means a relevant problem in finance. The dynamics describing the price of vanilla options when constant volatilities and interest rates are assumed, is governed by the Black-Scholes model, a linear parabolic partial differential equation with terminal value given by the pay-off of the option contract and no additional boundary conditions. Here, we present a digital quantum algorithm to solve Black-Scholes equation on a quantum computer by mapping it to the Schrödinger equation. The non-Hermitian nature of the resulting Hamiltonian is solved by embedding its propagator into an enlarged Hilbert space by using only one additional ancillary qubit. Moreover, due to the election of periodic boundary conditions, which are needed for an efficient diagonalization of the discretized momentum operator, we duplicate the initial condition, which substantially improves the stability and performance of the protocol. The algorithm shows a feasible approach for using Hamiltonian simulation techniques to solve the price dynamics of financial derivatives on a digital quantum computer. Our approach differs from those based on Monte Carlo integration, exclusively focused on sampling the solution assuming the dynamics is known. Assuming a bounded truncation error, our algorithm remarkably provides an exponential speedup with respect to classical numerical methods when simulating the dynamics, reducing the complexity from $O(2^n)$ to $O(\text{poly}(n))$. We report expected accuracy levels comparable to classical numerical algorithms by using 10 qubits and 94 entangling gates to simulate its dynamics on a fault-tolerant quantum computer, and an expected success probability of the post-selection procedure due to the embedding protocol above 60%.

I. INTRODUCTION

In finance, European-style vanilla options are financial derivative contracts written on an underlying asset, which give the holder the right to buy or sell such asset on a specified future date at a predetermined strike price. One of the fundamental tasks of quantitative finance is to calculate a *fair price* of such option contract before its expiration time. This task is far from being straightforward due to the randomness associated to the time evolution of both the underlying stock and the interest rates, whose dynamics can be modelled via either a stochastic processes or a partial differential equation (PDE), both connected by the celebrated Feynman-Kac formula. One of the first successful approaches to this problem was achieved by F. Black and M. Scholes in 1972, who proposed the celebrated Black-Scholes model [1], in which a log-normal distribution of the underlying stock price is assumed. Even though a closed-form solution exists for this dynamics, the numerical method proposed in this manuscript relies on the Black-Scholes model in order to show its properties of convergence and performance. Moreover, we show that this method is also applicable to time-dependent volatility PDEs, for which non closed-form solution exists in general. Additionally, the scope of this paper is to present a novel algorithm thought to be extended to more complex PDEs as a future work. Besides, numerical solutions also turn out to be fundamental when hedging a portfolio with a great number of coupled options. Several classical methods proposed in the literature include finite differences, finite elements, Monte Carlo methods, and Fourier (spectral) methods [2–6].

Quantum technologies have experienced a rapid development in the last decade. Recently, Google has achieved quantum advantage, meaning that they have performed a calculation employing a superconducting processor faster than the most powerful supercomputers available today [7]. One of the fields which will expectably experience a deep impact due to this upcoming technology is finance. Indeed, the emergence of scalable quantum technologies will affect forecasting, pricing and data science, and will undoubtedly have an economic impact in the following years [8, 9]. Certainly, there already exist several efforts in this direction, for instance, an attempt to predict financial crashes [10, 11], the application of the principal component analysis to interest-rate correlation matrices [12], quantum methods for portfolio optimization [13–17], quantum generative models for finance [18], a quantum model for pricing collateral debt obligations [19], a protocol to optimize the exchange of securities and cash between parties [20] and an application to improve Monte Carlo methods in risk analysis [21, 22], among many others.

Regarding the option pricing problem, it has been studied the problem of sampling the solution resulting from the stochastic process of the Black-Scholes model by employing Monte Carlo methods, and assuming its dynamics is known

* Corresponding author: javier.gonzalezc@ehu.eus
† Corresponding author: mikel.sanz@ehu.eus

at any maturity time. In Ref. [23], the authors proposed a theoretical approach to sample the solution of the stochastic process using quantum Monte Carlo integration, reporting a quadratic speedup versus classical sampling techniques. Afterwards, an experimental implementation in the IBM Tokyo quantum processor was attained in Refs. [24–26], employing a gate-based methodology to price options and portfolios of options. More recently, another approach to solve the stochastic process was proposed in [27], where a unary representation of the asset value is used to build a quantum algorithm for European-style option pricing. Another relevant alternative perspective to deal with pricing problems involving linear partial differential equations consists in adapting quantum algorithms applied to existing quantum numerical solvers [28–30].

In this Article, we propose a quantum algorithm for solving the dynamics of the Black-Scholes partial differential equation on a quantum computer. We map Black-Scholes equation into the Schrödinger equation, which results into a non-Hermitian Hamiltonian. Additionally we impose periodic boundary conditions to achieve an efficient diagonalization of the discretized momentum operator into a quantum computer. In order to simulate the non-unitary dynamics in a quantum processor [31–37], we embed the time propagator into an enlarged Hilbert space, making use of only one ancillary qubit. Thanks to this embedding we can post-select the result depending on the outcome of the ancillary qubit, which allows us to reproduce the dynamics of the non-Hermitian Black-Scholes Hamiltonian. Moreover, by introducing a second ancillary qubit, we duplicate the initial boundary condition to fit the periodic boundary conditions, leading to an improvement of the performance, accuracy and stability of the algorithm by mitigating edge effects propagation. In comparison with classical methods, our algorithm remarkably provides an exponential speedup versus numerical classical techniques when solving the dynamics of the Black-Scholes partial differential equation, since the number of terms in the Hamiltonian can be truncated with a polynomial number of terms while keeping the error bounded, and consequently reducing the complexity from $O(2^n)$ to $O(\text{poly}(n))$, with n the number of qubits. After benchmarking our algorithm for a wide range of financial parameters, the simulations show a precision comparable to classical algorithms with a quantum circuit comprising 10 qubits and 94 entangling gates to simulate dynamics of the PDE in a fault-tolerant quantum computer, and furthermore, an expected success probability of the post-selection protocol above 60%.

The article is structured as follows. First, we briefly review the Black-Scholes model. Then, we propose an embedding protocol and present the digitalization of the space used to encode the problem into a digital quantum computer. Next, we provide the details of our algorithm and depict its circuit implementation. Finally, we show the results and discuss the future scopes.

II. BLACK-SCHOLES SCHRÖDINGER EQUATION

Under the assumption of constant interest rate and volatility, and provided certain ideal market conditions, Black-Scholes model [1] is based on the possibility of building a perfect dynamic hedging portfolio strategy, known as *delta hedging*, which consists in holding, at each time, a number of shares equal to the derivative of the option price with respect to stock price. Therefore, the only risky (random) factor associated to portfolio dynamics is eliminated and the value of the portfolio agrees with the option value at any time. The pricing problem for a specific derivative contract, i.e. to determinate its present price $V(t = 0, S)$, is given by the Black-Scholes PDE,

$$\frac{\partial V}{\partial t} + rS\frac{\partial V}{\partial S} + \frac{1}{2}\sigma^2 S^2 \frac{\partial^2 V}{\partial S^2} = rV, \tag{1}$$

together with the terminal condition for the price of the option given by the pay-off of the option contract, $V(t = T, S)$, defined at maturity time, T, for any plausible value of the underlying stock $S \geq 0$ and on the strike price, K. Here, r represents the constant risk-free interest rate while σ is the constant volatility of the stock, both assumed to be constant. In the case of a European Put-type option, the pay-off function reads $V_p(T, S) = \max\{K - S, 0\}$.

Black-Scholes equation has a similar structure to Schrödinger equation [38], which suggests the possibility of simulating such model in a quantum platform. To that end, we rewrite the Black-Scholes equation in a Hamiltonian form. First, the change of variables $S = e^x$, $-\infty < x < \infty$, allows us to recover the unbounded position variable, leading to the equation

$$\frac{\partial V}{\partial t} + \left(r - \frac{\sigma^2}{2}\right)\frac{\partial V}{\partial x} + \frac{\sigma^2}{2}\frac{\partial^2 V}{\partial x^2} = rV. \tag{2}$$

Note that this equation is a backward parabolic equation. Thus we can reverse time $t \to \tau = T - t$, obtaining a forward

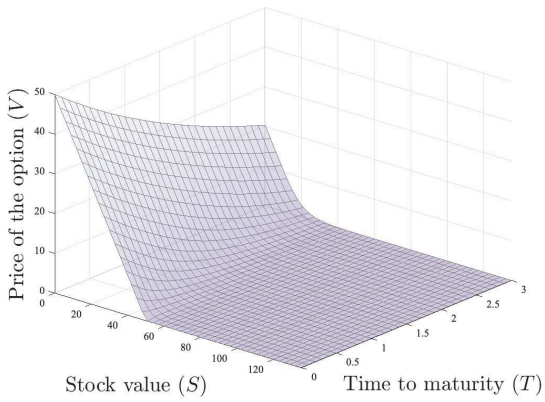

FIG. 1. Typical solutions of Eq. (1) for a European Put-type option. Simulation parameters: $S_{\max} = 135$ u, $K = 50$ u, $\sigma = 0.2$ and $r = 0.3$.

parabolic equation, and consequently an initial value problem where $V_p(\tau = 0, S) = \max\{K - S, 0\}$.

Finally, let us also introduce the momentum operator $\hat{p} := -i\frac{\partial}{\partial x}$ to rewrite Eq. (1) as

$$\frac{\partial V}{\partial \tau} = i\hat{H}_{BS} V \tag{3}$$

where we define

$$\hat{H}_{\text{BS}} = i\frac{\sigma^2}{2}\hat{p}^2 - \left(\frac{\sigma^2}{2} - r\right)\hat{p} + ir\mathbb{I}. \tag{4}$$

as the Black-Scholes Hamiltonian. Solutions to Eq. (3) are given by the time propagator $\hat{U}(\tau) = e^{i\tau\hat{H}_{BS}}$ acting on the initial condition.We can observe in Eq. (4) that the Black-Scholes Hamiltonian is a non-Hermitian operator, i.e., $\hat{H}_{BS} \neq \hat{H}^{\dagger}_{BS}$, which implies that neither its eigenvalues are necessarily real, nor the associated time propagator, $\hat{U}(\tau)$, is unitary. The evolution of a closed quantum system is always unitary and hence, this fact supposes a major drawback in terms of finding a physical system that evolves following the dynamics given by Black-Scholes model. To tackle this issue, we embed the propagator into a larger space (Section III), employing afterwards a post-selection technique (Section V E) so that we effectively retrieve the desired Black-Scholes dynamics.

III. EMBEDDING PROTOCOL

The Black-Scholes Hamiltonian, Eq. (4), can be decomposed into a Hermitian and an anti-Hermitian part, i.e. $\hat{H}_{\text{BS}} = \hat{H}_{\text{BSH}} + \hat{H}_{\text{BSA}}$, with

$$\hat{H}_{\text{BSH}} = -\left(\frac{\sigma^2}{2} - r\right)\hat{p}, \quad \hat{H}_{\text{BSA}} = i\left(\frac{\sigma^2}{2}\hat{p}^2 + r\mathbb{I}\right). \tag{5}$$

Additionally, we have that $[\hat{H}_{\text{BSH}}, \hat{H}_{\text{BSA}}] = 0$, so via the Baker–Campbell–Hausdorff formula [39], the propagator can be written as $\hat{U}(t) = e^{i\tau\hat{H}_{\text{BSA}}}\, e^{i\tau\hat{H}_{\text{BSH}}}$. Furthermore, notice that $\hat{O}(\tau) = e^{i\tau\hat{H}_{\text{BSA}}}$ is an Hermitian operator.

In order to circumvent the problem of dealing with the non-Hermitian operator, we embed the propagator $\hat{O}(\tau)$ into a larger unitary operator using a technique from operator theory called *unitary dilation* [40]. Indeed, by adding an ancillary qubit, q_E, to our system, we can embed $\hat{O}(\tau)$ into the unitary operator $\tilde{U}(\tau)$ which can be written as

$$\tilde{U}(\tau) = \begin{pmatrix} \hat{O} & \sqrt{1-\hat{O}^2} \\ \sqrt{1-\hat{O}^2} & -\hat{O} \end{pmatrix} = \left(\hat{\sigma}^z_E \otimes \mathbb{I}\right) \exp\left(i\hat{\sigma}^y_E \otimes \tilde{H}(\tau)\right), \tag{6}$$

with $\tilde{H}(\tau) = \arccos(\hat{O}(\tau))$ the 'integrated embedded Hamiltonian' and $\left\|\hat{O}(\tau)\right\| \leq 1$.

Starting from the initial state $|\Phi_0\rangle = |0_E\rangle \otimes \left|V_p\right\rangle$, with $\left|V_p\right\rangle$ encoding the pay-off condition of the PDE, the system evolves according the unitary operator $\tilde{U}(t)$ to obtain the final state

$$|\Phi\rangle = \hat{O}\,|0_E\rangle \otimes \left|V_p\right\rangle + \sqrt{1-\hat{O}^2}\,|1_E\rangle \otimes \left|V_p\right\rangle. \tag{7}$$

If we apply a post-selection technique filtering the outcomes with the ancillary qubit in the state $|0_E\rangle$, we can simulate the propagator $\hat{O}(\tau)$ into a quantum computer, and in consequence, the whole Black-Scholes Hamiltonian dynamics. We provide the details of the state preparation and post-selection process in Section V.

IV. DIGITIZATION OF THE SPACE

In order to perform a digital simulation of the Black-Scholes equation using a quantum computer, it is required a discretization of position and momentum spaces based on the number of qubits employed. The possibility of simulating the Black-Scholes model on a discretized space is guaranteed by the Nyquist-Shannon sampling theorem [41] (see and Appendix VII A for details). Following the work in Ref. [42], a wave function $|\Psi\rangle$ such that $|\Psi(x)| < \epsilon$ when $|x| > L$ and whose Fourier transform $|\hat{\Psi}(p)| < \epsilon$ if $|p| > L$ can be sampled in position space using the basis of sampling vectors $\{\left|x_j\right\rangle\}$ where $x_j = -L + j\delta_x$, with $\delta_x \leq \frac{\pi}{L}$ and $j = 0, 1, ..., N_x - 1$ such that $x_j \in [-L, L]$. For a given interval, in the limit where $\delta_x = \frac{\pi}{L}$, the minimum N_x is given by the equality $2L = \delta_x(N_x - 1)$. Hence, the wave function can then be rewritten as $|\Psi\rangle = \sum_{j=0}^{N_x-1} \Psi(x_j)\left|x_j\right\rangle$. The conjugate momentum basis is obtained by the discrete Fourier transform of the position basis, $\text{QFT} : \left|x_j\right\rangle \mapsto \left|p_j\right\rangle = \frac{1}{\sqrt{N}} \sum_{k=0}^{N-1} \omega_{N_x}^{jk} |x_k\rangle$, where $\omega_{N_x} = e^{\frac{2\pi i}{N_x}}$. We denote the discrete quantum Fourier transform matrix operator as $\hat{F}$. These two sampling basis allow us to define the following discretized position and momentum operators acting on their own basis as $\hat{X}_x\left|x_j\right\rangle = x_j\left|x_j\right\rangle$ and $\hat{P}_k\,|p_k\rangle = p_k\,|p_k\rangle$.

For a space spanned by n qubits, they generate $N_x = 2^n$ basis states (grid points), which means an exponential compression of the grid with respect to any numerical classical algorithm. This fact leads to an exponential speed up versus

Algorithm	Complexity
Quantum Simulation	$O(\text{poly}(n))$
Finite differences (explicit)	$O(T_{\text{steps}} 2^n)$
Finite differences (Crank-Nicolson)	$O(T_{\text{steps}} 2^n)$
Fast Fourier transform	$O((n+1)2^n)$
Matrix exponentiation	$O(2^n)$

TABLE I. Algorithms and their costs [43] for solving the Black-Scholes PDE. We compare the costs of different tasks when working with multivariate functions, from the construction of the state, to the simulation of their evolution. ϵ, desired error bound; n, the number of qubits, equivalent to having 2^n degrees of freedom (points in the grid); and T_{steps}, the number of time steps

numerical classical techniques if we can simulate the dynamics of the system employing a polynomial number of gates in terms of the number of qubits, incurring in a complexity $O(\text{poly}(2^n))$. On the other hand, by contrast, numerical methods incur into an exponential cost to simulate the dynamics of the PDE on a 2^n points grid, see Table I.

We consider an equispaced grid of the interval $[-L, L]$, thus, the position space is discretized into the values $x = -x_{\max} + \delta_x \beta_x$, with $\delta_x = \frac{2x_{\max}}{N_x - 1}$ and $\beta_x = 0, \ldots, N_x - 1$. If we consider that the position $x = -x_{\max}$ is represented by the state $|-x_{\max}\rangle = |0...0\rangle$, and the position $x = x_{\max}$ is represented by $|x_{\max}\rangle = |1...1\rangle$, the matrix form of this operator in the x basis results

$$\hat{X}_x = x_{\max} \begin{pmatrix} -1 & 0 & \ldots & 0 & 0 \\ 0 & -1+\delta_x & \ldots & 0 & 0 \\ \vdots & \vdots & \ddots & \vdots & \vdots \\ 0 & 0 & \ldots & 1-\delta_x & 0 \\ 0 & 0 & \ldots & 0 & 1 \end{pmatrix}. \tag{8}$$

Let us now construct the momentum operator, $\hat{p}$. By using the second order of finite differences, we approximate the derivative of a certain function as

$$\frac{d\mathrm{f}(x)}{dx} \approx \frac{\mathrm{f}(x+\delta_x) - \mathrm{f}(x-\delta_x)}{2\delta_x}. \tag{9}$$

Consequently, imposing periodic boundary conditions, the discrete momentum operator in the position basis is given by the matrix

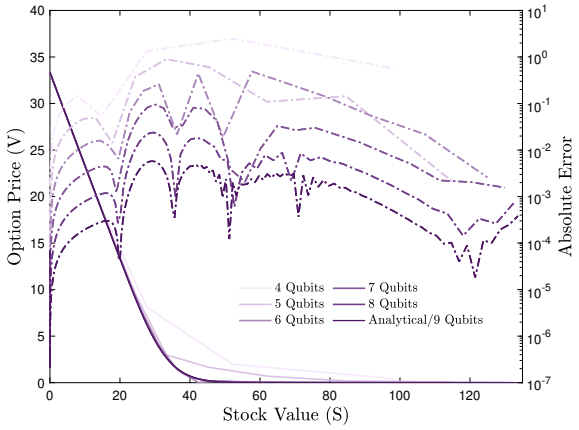

FIG. 2. Continuos line: convergence of the solution of Black-Scholes put option pricing problem obtained with the finite differences discretized operator $\hat{P}_x$ for distinct number of qubits, $n = 1 \ldots 8$ (excluding ancillary qubits and the one used to duplicate the initial condition) and the analytical solution. Dashed line: discretization error per point depending on the number of qubits, $n = 1 \ldots 9$ (excluding ancillary qubits and the one used to duplicate the initial condition). Simulation parameters: $S_{\max} = 135$ u, $K = 50$ u, $\sigma = 0.2$, $r = 0.3$, $T = 1$ year.

$$\hat{P}_x = \frac{-i}{2\delta_x} \begin{pmatrix} 0 & 1 & 0 & \ldots & 0 & -1 \\ -1 & 0 & 1 & \ldots & 0 & 0 \\ \vdots & \vdots & \vdots & \ddots & \vdots & \vdots \\ 0 & 0 & \ldots & -1 & 0 & 1 \\ 1 & 0 & \ldots & 0 & -1 & 0 \end{pmatrix}. \tag{10}$$

Thanks to the choice of periodic boundary conditions, the momentum matrix $\hat{P}_x$ belongs to circulant matrix class, and therefore its diagonal form is obtained by using the discrete Fourier transform unitary matrix, i.e.

$$\hat{P}_k = \hat{F}_{N_x} \hat{P}_x \hat{F}^{\dagger}_{N_x}. \tag{11}$$

This transformation can be efficiently implemented in a quantum computer [44]. Otherwise we can not ensure the efficient diagonalization of the momentum matrix, incurring into an exponential cost in the general case. The analytical expression of the eigenvalues of $\hat{P}_x$ is also known, and is described by the equation

$$p_k = \frac{\sin\left(\frac{2\pi k}{N_x}\right)}{\delta_x}, \quad k = 0 \ldots N_x - 1. \tag{12}$$

This diagonal form obtained via the quantum Fourier transform simplifies considerably the implementation of the momentum operator, as all the terms of the decomposition of the operator in the Pauli basis commute among them.

In Fig. 2, we illustrate the convergence of the solution to Black-Scholes equation and its relative discretization error with respect to the analytical solution for different number of qubits obtained by making use of the discrete operators $\hat{X}_x$ and $\hat{P}_k$.

V. QUANTUM CIRCUIT IMPLEMENTATION

In this section, we show the different components of the circuit which simulates the price evolution for a put option contract in a quantum computer; the procedure for a call option would be similar but initializing the process in the corresponding pay-off state. We depict a general overview of the quantum circuit of $n + 2$ qubits in Fig. 3. In the following sections we present a detailed explanation of every block of the circuit.

A. Boundary Conditions and Initial state

As introduced in section II, the pricing problem of an European put option is given by Black-Scholes PDE and the boundary condition depending on the strike price, K, at maturity time, $\tau = 0$,

$$V_p(\tau = 0, S) = \max\{K - S, 0\}. \tag{13}$$

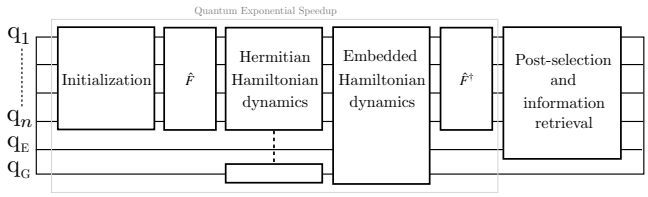

FIG. 3. General overview of the circuit that accomplish Black-Scholes digital simulation. In the first step of the circuit, we obtain the initial state which encodes the payoff condition of the corresponding option type. Then, we apply the quantum Fourier transform, $\hat{F}$, that enables us to work in the momentum space. We implement both sets of gates from Hermitian and non-Hermitian dynamics using an ancillary qubit q_G. In the case of non-Hermitian dynamics, an embedding qubit, q_E, is also required. In order to recover the information in position space, we operate with inverse quantum Fourier transform and, in the end, we perform the measure and post-selection protocol.

Additionally, due to the choice of periodic boundary conditions for momentum operator in Eq. (10), we make use of one of the n qubits to duplicate the initial condition in the x space in order to mitigate border effects. The solution to the financial problem is then given in the interval $(-x_{\max}/2, x_{\max}/2)$. In the case of the European put option, these assumptions are translated into the following encoding of the pay-off initial state

$$\left|V_p\right\rangle = \sum_{j=0}^{N_{\max}} \frac{K - e^{-x_{\max}/2 + j\delta_x}}{\Lambda^{1/2}} \left(\left|x_j\right\rangle + \left|x_{N_x-1-j}\right\rangle\right), \tag{14}$$

with

$$N_{\max} = \left\lfloor (N_x - 1)\left(\frac{\log(K)}{2x_{\max}} + \frac{1}{4}\right)\right\rfloor \quad \text{and}$$
$$\Lambda = \left(2\sum_{m=0}^{N_{\max}} (K - e^{-x_{\max}/2 + m\delta_x})^2\right). \tag{15}$$

Moreover, we need two additional ancillary qubits, q_E and q_G, associated with the embedding and the optimal implementation in terms of entangling quantum gates respectively. Thus, the initial state of the embedded system results $|\Phi_0\rangle = |0_G\rangle \otimes |0_E\rangle \otimes \left|V_p\right\rangle$.

In the general case, loading an arbitrary state into a quantum computer requires an exponential quantity of gates [45–51], which is inefficient and destroys any possible quantum advantage in the dynamics simulation. Nevertheless, for some specific cases such as smooth differentiable functions, the initial state can be efficiently loaded into a gate-based quantum computer, as detailed in [43, 52]. In Ref. [43] the author proved a requirement of an exponentially small entanglement entropy for each added qubit to represent this kind of functions, and consequently in the number of two-qubit gates demanded. The work presented in Ref [52] introduces two algorithms to achieve the efficient approximated loading of some functions, which in particular includes the initial state of the European Put options.

B. Quantum Fourier Transform

As Black-Scholes Hamiltonian only depends on the momentum operator $\hat{P}_x$, we can employ the quantum Fourier transform, Fig. 4, to change from the position basis, encoding the initial state, to the momentum basis, which simplifies the implementation of the dynamics in terms of the circuit depth. Indeed, we aim to simulate the operators $\hat{O}(\tau)$ and $e^{i\tau\hat{H}_{\text{BSH}}}$. By using Eq.(11) and the identity, $f\left(\hat{F}^\dagger_{N_x}\hat{P}_k\hat{F}_{N_x}\right) = \hat{F}^\dagger_{N_x} f\left(\hat{P}_k\right)\hat{F}_{N_x}$, where f is an analytic function, the problem reduces itself to calculate the exponential of operator functions acting on diagonal momentum matrices. In this way, an initial Quantum Fourier transform, $\hat{F}$, allows us to transform the initial condition encoded in the positions basis, Eq. (13), into the momentum space. After applying the diagonal operators, the inverse Fourier transform, $\hat{F}^\dagger$ enables us to recover the solution in position space, which encodes the price information. Therefore, we can assume from now on that the operators are diagonal and that the complexity of the quantum Fourier transform, $O(n\log n)$, does not play a decisive role in the global complexity of the algorithm as it scales polynomially with the number of qubits [53].

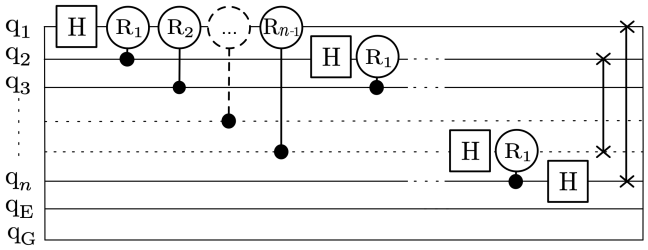

FIG. 4. The circuit of the quantum Fourier transform, $\hat{F}$, for n qubits. Once we have performed all the controlled rotations, it is necessary to swap all the qubits in order to retrieve the initial indexing in the momentum space. The used logic gate R_m corresponds to the control phase gate $R(\phi = \frac{\pi}{2^m})) = \text{diag}(1, 1, 1, \exp(i\phi))$.

C. Gates of Hamiltonian dynamics

Once we have the expression for the eigenvalues of $\hat{P}_k$, Eq. (12), we rewrite both Hamiltonians $\hat{H}_{\text{BSH}}$ and $\tilde{H}$ in the Cartan subalgebra basis. This allows us to find the logic gates to implement the corresponding qubit operators. Let us first focus on the non-Hermitian part, $\tilde{H}$. The integrated Hamiltonian of the embedded time evolution operator, $\hat{O}(\tau)$, is given by

$$\tilde{H} = f\left(-T\left(\frac{\sigma^2}{2}\hat{P}_k^2 + r\mathbb{I}\right)\right), \tag{16}$$

where $f(x) = \arccos(\exp(x))$. Hence, we can use the spectral theorem to decompose the Hamiltonian into projectors basis

$$\tilde{H} = \sum_{k=0}^{N_x-1} \underbrace{f(-T(\frac{\sigma^2}{2}p_k^2 + r))}_{\tilde{h}_k} |p_k\rangle\langle p_k|, \tag{17}$$

where p_k is given by Eq. (12). For the case of the Hermitian Hamiltonian, the decomposition corresponds to

$$\hat{H}_{\text{BSH}} = \sum_{k=0}^{N_x-1} \underbrace{-\left(\frac{\sigma^2}{2} - r\right) p_k}_{h_k} |p_k\rangle\langle p_k|. \tag{18}$$

By rewriting $\hat{P}_k$ in terms of the Cartan basis, $\hat{c}_I$, we obtain

$$\tilde{H} = \sum_{i_0 \ldots i_{n-1}=0}^{1} \underbrace{\left(\frac{1}{N_x}\sum_{k=0}^{N_x-1} \tilde{h}_k W_I\left(\frac{k}{N_x}\right)\right)}_{\tilde{h}'_I} \underbrace{\hat{\sigma}_0^{i_0} \ldots \hat{\sigma}_{n-1}^{i_{n-1}}}_{\hat{c}_I}, \tag{19}$$

and

$$\hat{H}_{\text{BSH}} = \sum_{i_0 \ldots i_{n-1}=0}^{1} \underbrace{\left(\frac{1}{N_x}\sum_{k=0}^{N_x-1} h_k W_I\left(\frac{k}{N_x}\right)\right)}_{h'_I} \underbrace{\hat{\sigma}_0^{i_0} \ldots \hat{\sigma}_{n-1}^{i_{n_1}}}_{\hat{c}_I}, \tag{20}$$

where $\hat{\sigma}_j^0 = \mathbb{I}_j$, $\hat{\sigma}_j^1 = \hat{\sigma}_j^z$ denotes the operator acting on qubit j, $j = 0, ..., n-1$, and $W_I(x)$ is the I-th Walsh function with $I = \sum_{j=0}^{n-1} i_j 2^j$, and h'_I, $\tilde{h}'_I$ the coefficients of the decomposition in the Cartan basis (see Appendix VII C).

Notice now that from this decomposition we can appreciate that the product $\hat{\sigma}_E^y \otimes \tilde{H}$ is given by a sum of commuting Pauli observables, so by using the Baker–Campbell–Hausdorff [39] formula it is straightforward to show that its exponential can be divided into a product of single exponentials, Eq. (21).

$$U = e^{i\beta\, \hat{\sigma}_E^y \otimes (\hat{\sigma}_{i_1}^z \ldots \hat{\sigma}_{i_k}^z)}. \tag{21}$$

The same applies for the Hermitian Hamiltonian. In Fig. 5 we illustrate the gates needed to simulate this unitary operator [44].

D. Depth of the circuit

In the general case, the decomposition of each Hamiltonian in the Cartan basis leads to $N_x = 2^n$ multi-qubit interactions, which ranslated into logic gates in an optimized circuit, means $O(2^{n+1})$ entangling gates. Due to the symmetry (embedded Hamiltonian) and antisymmetry (Hermitian Hamiltonian) of the eigenvalues $\tilde{h}_k$ and h_k respectively, we can reduce the number of terms to 2^{n-1}. Unfortunately, this is still excessive and destroys any possible speedup versus numerical classical techniques. Therefore, the question addressed in this section is whether it is possible to truncate the number of terms up to a

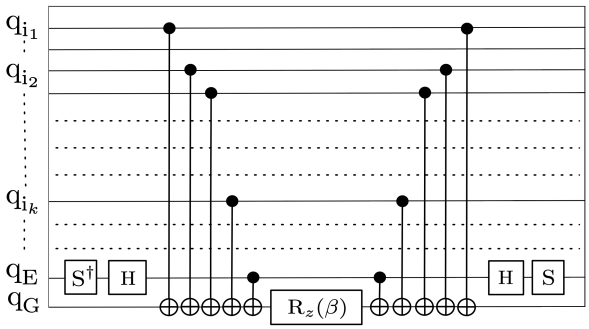

FIG. 5. Circuit implementation of operator in Eq. (21). The main idea behind this construction is to encode the parity of the involved qubits into the ancilla-gate qubit, q_G, so this qubit accomplish a rotation depending on that. The construction of the whole circuit involves as many of these terms as vectors of the Cartan basis are included in the decomposition of our Hamiltonian.

polynomial order without substantially affecting the accuracy of the algorithm.

Let us firstly focus on the Hermitian Hamiltonian since, as we will see at the end of this section, its truncation error dominates the total error. In this case, due to the antisymmetry of the eigenvalues, h_k, every non-zero term,h'_I, in the decomposition of the Hamiltonian in the Cartan basis, Eq. (20), must include $\hat{\sigma}_0^z$. For each non-zero term, the coefficients h'_I sum up to an analytical expression. We split the expressions into three categories: first qubit interaction, interactions including an odd number of bodies, and interactions with an even number of bodies. Denoting by $0 = j_0 < j_1 < ... < j_{2k} \leq n-1$ the indices of the qubits the operators act on, we obtain the reindexed coefficients,

$\underline{\hat{\sigma}_0^z\, \mathbb{I}_1 \ldots \mathbb{I}_{n-1}}$:

$$\frac{2^n - 1}{2^{n+1}} \frac{2r - \sigma^2}{x_{\max}} \cot\left(\frac{\pi}{2^n}\right). \tag{22}$$

$\underline{\hat{\sigma}_{j_0=0}^z \hat{\sigma}_{j_1}^z \ldots \hat{\sigma}_{j_{2k}}^z}$:

$$(-1)^k \frac{2^n - 1}{2^{n+1}} \frac{2r - \sigma^2}{x_{\max}} \cot\left(\frac{\pi}{2^n}\right) \tan\left(\frac{\pi}{2^{j_1+1}}\right) \ldots \tan\left(\frac{\pi}{2^{j_{2k}+1}}\right). \tag{23}$$

$\underline{\hat{\sigma}_{j_0=0}^z \hat{\sigma}_{j_1}^z \ldots \hat{\sigma}_{j_{2k-1}}^z}$:

$$(-1)^k \frac{2^n - 1}{2^{n+1}} \frac{2r - \sigma^2}{x_{\max}} \tan\left(\frac{\pi}{2^{j_1+1}}\right) \ldots \tan\left(\frac{\pi}{2^{j_{2k-1}+1}}\right). \tag{24}$$

where we define $\boldsymbol{J}$ as the index of the term corresponding to the indices of the qubits the operators act on.

We can check from Eqs. (23) and (24) that the arguments of the tangent functions verify $0 \leq \frac{\pi}{2^{j_l+1}} \leq \pi/4$ for $l = 1 \ldots 2k$. Hence, we have the inequality $\tan\left(\frac{\pi}{2^{j_l+1}}\right) \leq \frac{4}{2^{j_l+1}}$ due to the convexity of the tangent function. For a fixed n, considering the previous inequality, we obtain the upper bound

$$\tan\left(\frac{\pi}{2^{j_1+1}}\right) \ldots \tan\left(\frac{\pi}{2^{j_{2k}+1}}\right) \leq \frac{1}{2^{\sum_{l=1}^{2k}(j_l-1)}}. \tag{25}$$

Following the previous expression, let us now define the index $I'_n = \sum_{l=1}^{2k}(j_l - 1)$ for the terms which have an odd number of body interactions. Notice from Eqs. (23) and (24), that for every term with an even number of body interactions not ending in $\hat{\sigma}^z_{n-1}$, there exists a term with an odd number of body interactions ending in $\hat{\sigma}^z_{n-1}$ with the same coefficient value, hence this term inherits the index I'_n. To complete the assignment, we need to define the value of index I'_n for those terms with an even number of body interactions ending in $\hat{\sigma}^z_{n-1}$. For such purpose, we increase the number of qubits one unit, and consider the term as part of this system with a larger quantity of qubits not including the interaction with the last one, so we already know how to calculate its index in this scenario. To recover the index in the original system, consider then that the index of a term with an even number of body interactions increases one unit when the size of the system is increased in one qubit, it is $I'_{n+1}(\hat{\sigma}^z_{j_0=0}\hat{\sigma}^z_{j_1}...\,\hat{\sigma}^z_{j_{2k-1}}) = I'_n(\hat{\sigma}^z_{j_0=0}\hat{\sigma}^z_{j_1}...\,\hat{\sigma}^z_{j_{2k-1}}) + 1$. We conclude from Eq. (25) that with this reassignment if the index of a certain term is $I'_n(\boldsymbol{J}) = I'$, hence $|h'_{\boldsymbol{J}}|$ is upper bounded by $|h'_{\boldsymbol{J}}| \leq C/2^{I'}$, where C is a constant depending on n and the financial parameters ($C = \frac{2^n-1}{2^{n+1}}\frac{2r-\sigma^2}{x_{\max}}\cot\left(\frac{\pi}{2^n}\right)$). Notice that this reassignment is non-bijective, hence we denote $g_{I'}$ as the degeneration of the I'-th value of the index I'_n [54] (see Appendix VII E). We define M as the Mth largest value of the index I'.

We have now all necessary elements to prove that the error after truncating the first M index terms is exponentially supressed with M. Indeed, in order to quantify the error corresponding to the truncation from M-th term, we define the truncation error $\xi(M) = \left\| e^{iT\sum_{I'=M}^{\frac{n}{2}(n-1)-1}\sum_{\boldsymbol{J}|I'_n(\boldsymbol{J})=I'} h'_{\boldsymbol{J}}\hat{c}_{\boldsymbol{J}}} - e^{i\theta}\mathbb{I}\right\|_\infty$ (see Appendix VII E), where θ denotes the global phase gauge election and $\hat{c}_{\boldsymbol{J}}$ is the vector of the Cartan basis corresponding to the coefficient $h'_{\boldsymbol{J}}$ (notice that $\|\hat{c}_{\boldsymbol{J}}\|_\infty = 1\ \forall \boldsymbol{J}$). In the worst case scenario, the maximum rotation angle between two eigenstates corresponds to $\sum_{I'=M}^{\frac{n}{2}(n-1)-1}\sum_{\boldsymbol{J}|I'_n(\boldsymbol{J})=I'}|h'_{\boldsymbol{J}}| \leq C\sum_{I'=M}^{\frac{n}{2}(n-1)-1}\frac{g_{I'}}{2^{I'}} < \frac{2C'}{2^M}$, with C' a new constant depending on n and the financial parameters (see Appendix VII E). This rotation is evenly distributed, hence the optimal gauge choice is $\theta = 0$.

Consequently, taking M sufficiently large to guarantee that $C'/2^M \leq \pi/4$, we get the following upper bound for the truncation error

$$\xi(M) = \left\| e^{iT\sum_{I'=M}^{\frac{n}{2}(n-1)-1}\sum_{\boldsymbol{J}|I'_n(\boldsymbol{J})=I'} h'_{\boldsymbol{J}}\hat{c}_{\boldsymbol{J}}} - e^{i\theta}\mathbb{I}\right\|_\infty \leq \underbrace{\sqrt{2\left(1-\cos(2TC'/2^M)\right)}}_{C(M)}, \tag{26}$$

thus, if an error ϵ is allowed in our algorithm, we aim to find the minimum number of terms, M^ξ_ϵ, needed to guarantee that the truncation error $\xi(M^\xi_\epsilon) < \epsilon\ \forall M > M^\xi_\epsilon$. As the expression $C(M) = \sqrt{2\left(1-\cos(2TC'/2^M)\right)} \underset{M\to\infty}{\longrightarrow} 0$ monotonically, we can define $M^C_\epsilon = \max\{M|C(M) \geq \epsilon\}$.. Therefore $C(M^C_\epsilon) \geq \epsilon$, so $M^C_\epsilon \leq \log_2(2TC') - \log_2\left(\arccos\left(1-\epsilon^2/2\right)\right)$. As $C(M)$ is an upper bound for the truncation error, $\xi(M)$, we have that $M^\xi_\epsilon \leq M^C_\epsilon$, and consequently $M^\xi_\epsilon \leq \log_2(2TC') - \log_2(\arccos\left(1-\epsilon^2/2\right))$.

Finally, we show that the truncation error of the Hermitian Hamiltonian dominates the error. In the embedded case, we were not able to find analytic results for the sums defining the coefficients, but asymptotic expressions for large n, which are shown in Appendix VII D. Indeed, these expressions show that, for sufficiently large n, the Mth term of the embedded Hamiltonian is much smaller than the Mth term of the Hermitian Hamiltonian. Consequently, the truncation error of the former is upper bounded by the one of the other. As an illustration of these results, we have studied the case $n = 8$, since it already provides a discretization comparable to the standard classical case. For the case of $n = 8$, this analysis leads us to find an optimal truncation to implement the algorithm. We propose to use the largest 14 terms of the Hermitian Hamiltonian and the 6 largest of the embedded one, as this quantity of terms is the first local minimum of the truncation that provides an accurate enough solution. In terms of gates, it means 94 entangling gates to simulate its dynamics, which is feasible in current quantum processors [7]. The solution obtained is compared with the analytical solution in Fig. 6 (a). Also for $n = 8$, we show in Fig. 6 (b) that the terms of the Hermitian Hamiltonian are considerably larger than the embedded ones. Furthermore, we study all the possible combinations of truncations in Fig. 7, showing that the error strongly depends on the number of terms of the Hermitian Hamiltonian, and that therefore it dominates the dynamics.

E. Measurement and Post selection

Once the Hamiltonians have been simulated, the outcomes of the measurements in our circuit must be postselected in order to recover the non-Hermitian dynamics of Black-Scholes equation, which encodes the option price. Indeed, we firstly measure the ancillary embedding qubit. If it is $|0_E\rangle$, then we proceed to retrieve the price information, otherwise, we discard the measurement. The probability of recovering the desired dynamics when measuring the ancilla depends on the expression

$$Ps = \left\langle V_p\right| \hat{F}^\dagger e^{-2T(\frac{\sigma^2}{2}\hat{P}_k^2 + r\mathbb{I})}\hat{F}\left|V_p\right\rangle. \tag{27}$$

If the system has evolved following the desired dynamic, we retrieve the option price corresponding to the spot $\left|x_j\right\rangle$, which encodes the stock price of interest $S_j = e^{x_j}$, by measuring the POVM$\left\{\left|x_j\right\rangle\left\langle x_j\right|, \mathbb{I} - \left|x_j\right\rangle\left\langle x_j\right|\right\}$. This task is attained by using a multi-control gate acting on an extra qubit, in our case, we can use the ancilla q_G.

The success probability, Eq. (27), strongly depends on the maturity time and risk-free interest rate, but, for the usual range of financial parameters, its value is always above 0.6 as depicted in Fig. 8 (a). Therefore, we only need to double the number of runs of the algorithm, which does not change its polynomial behaviour. Assuming the constraint $e^{x_{\max}/2} = 3K$, it is possible to obtain a lower bound $Ps \geq e^{-2Tr}\gamma(N_x, K)$

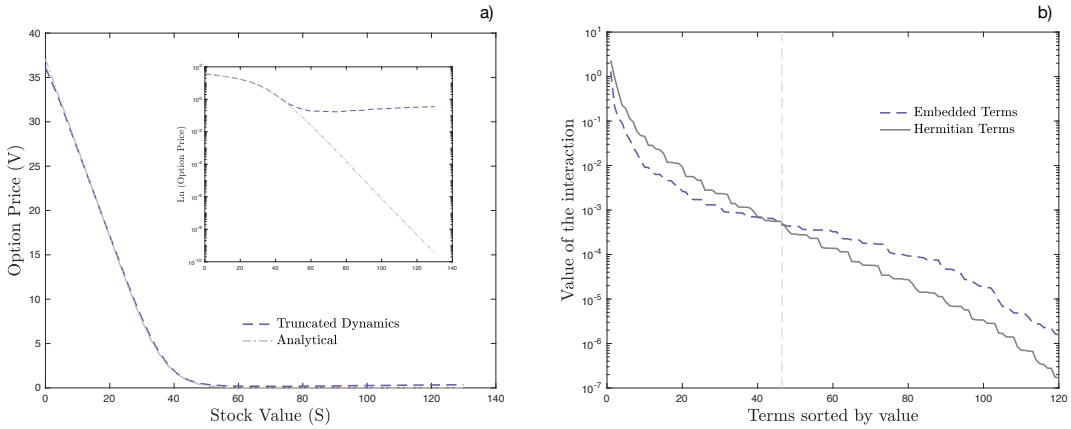

FIG. 6. (a) Solution to Black-Scholes equation obtained by evolving the truncated dynamics considering the largest 14 terms of the Hermitian Hamiltonian and the largest 6 interactions of the embedded. We compare it with the analytical solution evaluated in the same grid points. The inset shows both curves in a logarithmic scale, what enables us to appreciate the difference. (b) Hermitian and embedded interactions terms sorted by absolute value represented in a logarithmic scale. For the most significant values, Hermitian terms dominate over embedded ones. Simulation parameters: $n = 8$, $S_{\max} = 135$ u, $K = 50$ u, $\sigma = 0.2$, $r = 0.3$, $T = 1$ year.

(see Appendix VII H). The function $\gamma(N_x, K)$, depicted in Fig. 8 (b), shows an asymptotic behaviour when $N_x \to \infty$,

$$\lim_{N_x\to\infty} \gamma(N_x, K) = \frac{\left(-1 + K^2 - 6K^2\log(K)\right)^2}{(-1 + 12K^2 - 11K^4 + 36K^4\log(K))\log(3K)}. \tag{28}$$

Finally, the discrete value of solution for the Black-Scholes equation at maturity time, T, on the stock price $S_j = e^{x_j}$ is given by the expression

$$V_p(T, S_j) = \sqrt{p(x_j \cap 0_E)\Lambda}, \tag{29}$$

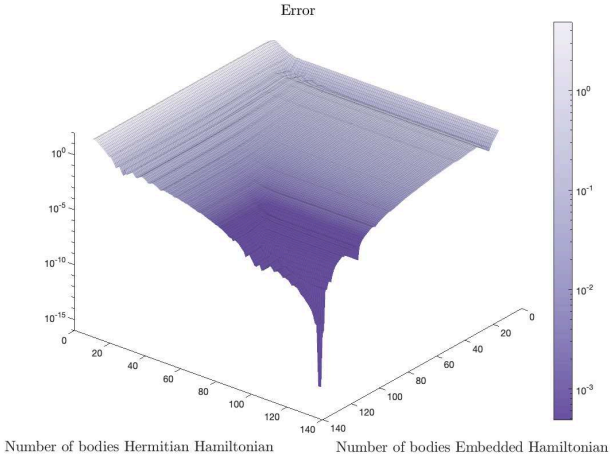

FIG. 7. Truncation error: Relative error of the approximated solution considering all the combinations of largest terms of the Hermitian and embedded Hamiltonian with respect to the analytical solution calculated via L^1-norm. Simulation parameters: $S_{\max} = 135$ u, $K = 50$ u, $\sigma = 0.2$, $r = 0.3$, $T = 1$ year, $n = 8$.

where $p(x_j \cap 0_E) = p(x_j|0_E)p(0_E) \geq 0.6p(x_j|0_E)$ is the probability of measuring the eigenstate $|x_j\rangle$ and the ancillary embedding qubit in the state $|0_E\rangle$, and Λ is given by Eq. (15).

F. Time and stock-price-dependent volatility

We have considered a constant volatility, but our algorithm is straightforwardly adaptable to introduce a time dependance in volatility. This fact allows us to reproduce more complex financial models such as Heath–Jarrow–Morton. In the general case time dependent volatility expression is given by an interpolation among equispaced known values. The introduction of this assumption means a slight change in the algorithm, the only difference in the coefficients decomposition is experimented in Eqs. (17) and (18) where the coefficient h_k and $\tilde{h}_k$ turn into $-\left(\frac{\frac{1}{T}\int_0^T \sigma^2(\tau)}{2} - r\right)p_k$ and $f\left(-\left(\frac{\int_0^T \sigma^2(\tau)}{2}p_k^2 + rT\right)\right)$ respectively. Thus, the mean value theorem for definite integrals guarantees that the average value $\bar{\sigma^2} = \frac{1}{T}\int_0^T \sigma^2(t)$ is lower and upper bounded. This enables us to focus our study only in a bounded interval for the volatility, as we have done by now.

Regarding the case of a stock price-dependent-volatility, we can introduce a perturbation $\sigma_1(\hat{x})$ of order ϵ around a constant value σ_0. The diagonalization of $\sigma_0\mathbb{I} + \epsilon\hat{\sigma}_1(\hat{x})$ can be obtained via quantum Fourier transform with a deviation of order ϵ in the eigenvalues, what enables us to continue applying our protocol while keeping the error bounded and an exponential speed up versus numerical classical techniques. We remark that, for this case there exists no analytical solution to the PDE, therefore our algorithm would provide a meaningful numerical solution. This case will be studied in detail in further works.

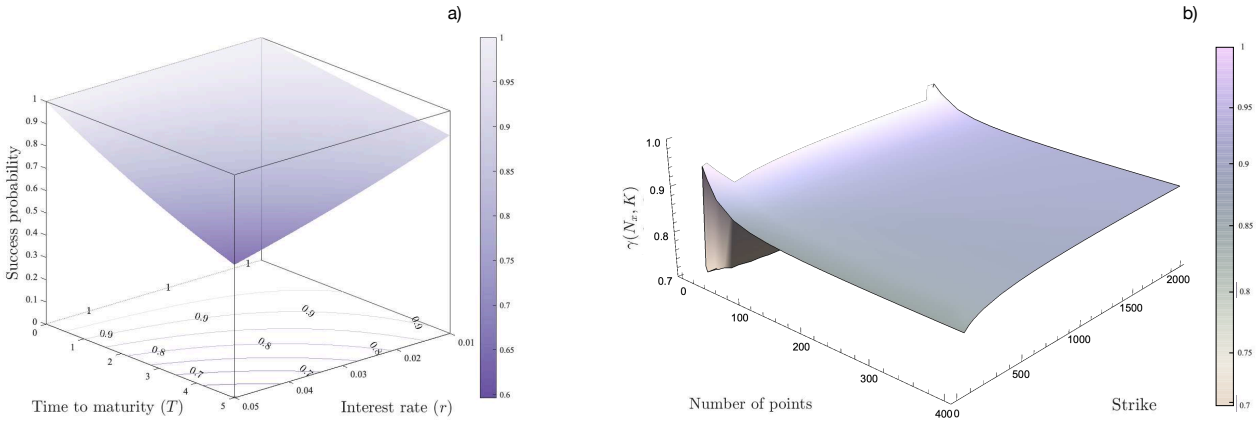

FIG. 8. (a) Success probability in post-selection protocol corresponding to Eq. (27) depending on time to maturity in years and risk-free interest rate. The probability is above 0.6 for all values in the mesh. (b) Lower bound probability of success $\gamma(N_x, K)$. As we can observe there exists an asymptotic convergence value for both, number of points and strike. The value of the asymptotic limit is over 0.6, what indicates that our protocol would be success in more than a half of the realizations. Parameters values: $S_{\max} = 150$ u, $K = 50$ u, $\sigma = 0.2$, $n = 8$.

VI. CONCLUSIONS

We have introduced a quantum algorithm to numerically solve Black-Scholes partial differential equation in a digital quantum computer by mapping it to Schrödinger equation. The non-Hermitian nature of the resulting Hamiltonian has been solved by embedding the dynamics into an enlarged Hilbert space, and by post-selecting the outcome of the simulation. As a consequence of choosing periodic boundary conditions for the discretized momentum operator, and in order to improve the stability and performance of our algorithm, we added an additional ancillary qubit to duplicate the initial condition. We have described the implementation of the dyanmics for a wide range of relevant financial parameters in terms of qubit operators and quantum gates. Even though the number of terms resulting from the decomposition of the Hamiltonian in the computational basis grows exponentially with the number of qubits, we have been able to identify that only a polynomial number of interactions plays a relevant role to achieve an accurate solution, providing a remarkable exponential speedup with respect to classical numerical methods when simulating the dynamics of the Black-Scholes PDE. Indeed, we have obtained a precision comparable to classical algorithms with a total of 10 qubits and 94 entangling gates to simulate the Black-Scholes dynamics in a fault-tolerant quantum computer and an expected success probability value for the post-selection protocol above 60%. Our perspective for a future work is to introduce gate errors associated to NISQ devices in order to analyze the realistic implementation in a near-term quantum platform. We want to highlight that the embedding techniques introduced may be extended to simulate the dynamics of the general non-Hermitian Hamiltonians and imaginary time evolution. This could allow us to introduce additional degrees of freedom in the model, e.g. spatial-time dependent volatility (stochastic local volatility) or coupled options. For instance, we could use the quantum principal component analysis raised in Ref. [12] together with coupled Black-Scholes models to address problems with coupled options. Moreover, the present work has been accomplish for the European option pricing problem, but it may be carried through simulate different kind of options, considering American and Asiatic options, for example.

ACKNOWLEDGEMENTS

We thank Bruno Candelas for useful discussions regarding the digital implementation. Authors acknowledge financial support from Spanish Government PGC2018-095113-B-I00 (MCIU/AEI/FEDER, UE), Basque Government IT986-16 and the QUANTEK project from ELKARTEK program (KK-2021/00070), Spanish Ramón y Cajal Grant RYC-2020-030503-I, UPV/EHU PhD Grant 20/276, as well as from QMiCS (820505) and OpenSuperQ (820363) of the EU Flagship on Quantum Technologies, EU FET Open Grant Quromorphic (828826), EPIQUS (899368) and Shanghai STCSM (Grant No. 2019SHZDZX01-ZX04) . This work is supported by the U.S. Department of Energy, Office of Science, Office of Advanced Scientific Computing Research (ASCR) quantum algorithm teams program, under field work proposal number ERKJ333.

VII. APPENDIX

A. Nyquist-Shannon sampling Theorem

Nyquist-Shannon sampling Theorem [41] is a central part of our method, and has a remarkable importance in signal processing, communications, and data compression [55–57].

Theorem VII.1 (Nyquist-Shannon sampling). *Let $F(x) : \mathbb{R} \to \mathbb{R}$ be a real function that has support in $x \in [0, x_{max}]$ in position space and between $k = -k_{max}$ and $k = +k_{max}$ in momentum space. Consider a discrete sampling of $F(x)$ over the interval $x \in [0, L]$ with $L > x_{max}$ and at intervals of $\delta_x < \frac{\pi}{k_{max}}$. Then the theorem ensures that $F(x)$ can be reconstructed up to corrections that are exponentially small.*

Under some assumptions, the theorem allows us to reconstruct a function via discretization introducing only exponentially small errors, as long as the function is sampled in both momentum and position space over the whole region where it has support. Nevertheless, there is a constraint arising from the theorem. The lattice spacing x must be small enough in order to discretize states with high momentum. The theorem also requieres that the functions we want to simulate should be restricted to some area in both momentum and position space.

B. Initial State

When solving the Black-Scholes equation Eq. (1) after the change of variables $x = \log S$, the resulting equation, Eq. (2), turns out to be spatially homogeneous with respect to x, i.e. a partial differential equation with constant coefficients. In particular, this means that we can displace the initial condition by a given shift and solve the problem, in the sense that the actual solution of the original problem can be recovered afterwards by performing the same shift in the opposite direction. Indeed, given a bounded interval for the stock price $S \in [1/S_{max}, S_{max}]$, we make use of this property in order to have a symmetric initial condition with respect to x as follows: we make a shift in order to translate the initial condition of the Put such that the support of this initial condition is the interval $[0, 2\log S_{max},]$, instead of $[-\log S_{max}, \log S_{max}]$, for the given discretization. After this shift, we make a reflection in order to obtain periodic boundary conditions.

Black-Scholes initial value problem starts from the final payoff as initial condition. In terms of x, this condition results

$$V_p(T, x) = max\{K - \exp(x), 0\}. \tag{30}$$

Assuming that we use n qubits to discretize x, hence we have $N_x = 2^n$ points (eigenstates $|x_j\rangle$), each one of them corresponding to a discrete value of x_j.

$$x_j = -x_{\max} + \delta_x j \quad j = 0 \dots N_x - 1, \tag{31}$$

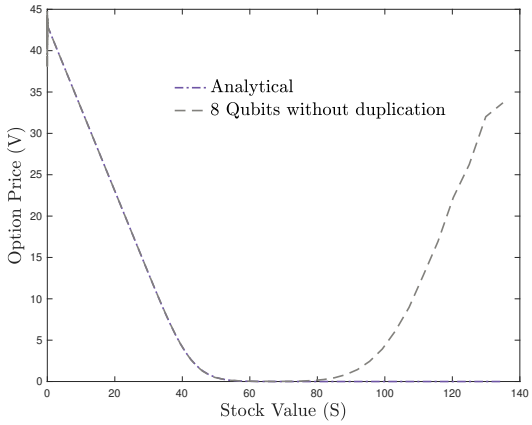

FIG. 9. Solution to the Black-Scholes equation without duplicating the initial condition. We can appreciate how it presents a strong border effect due to periodic boundary conditions. Simulation parameters: $n = 8$, $S_{\max} = 135$ u, $K = 50$ u, $\sigma = 0.2$, $r = 0.3$, $T = 1$ year.

$$\hat{X}\,|x_j\rangle = x_j\,|x_j\rangle \quad j = 0 \dots N_x - 1, \tag{32}$$

where $\delta_x = \frac{2x_{\max}}{N_x - 1}$. Now we have to find which is the largest index i such that $K - \exp(x_j) \geq 0$, we call this value $N_{\max}$

$$K - \exp(x_{N_{\max}}) = 0 \to \underbrace{-x_{\max} + \delta_x N_{\max}}_{x_{N_{\max}}} = \log(K), \tag{33}$$

hence

$$N_{\max} = \left\lfloor (N_x - 1)\left(\frac{\log(K)}{2x_{\max}} + \frac{1}{2}\right)\right\rfloor. \tag{34}$$

To encode this information into the quantum state, we associate the normalized and discretized value of the initial condition $C(T, x_j)$ to the probability amplitude of the corresponding eigenstate $|x_j\rangle$. Therefore, except normalization of the wave function, the coefficient (probability amplitude) of the eigenstate $|x_j\rangle$ is

$$K - \exp\left(-x_{\max} + \delta_x j\right)$$

for $j = 0....N_{\max}$.

If we now use one of the n qubits to duplicate the initial condition, then we have to consider some aspects. With this duplication we are mitigating the border effects that would appear if we do not duplicate the initial condition due to the choice of periodic boundary conditions, see Fig. 9. To accomplish the duplication we impose symmetry of the wave function with respect to $x = 0$, hence

$$\text{coefficient}(|x_j\rangle) = \text{coefficient}(|x_{N_x - 1 - j}\rangle) \quad \forall j = 0....N_x - 1. \tag{35}$$

Furthermore, this duplication reduces the size of the real price simulation space to the interval $(-x_{\max}/2, x_{\max}/2)$, which is

shifted to the interval $(-x_{\max}, 0)$, as we pursue to duplicate the initial condition with respect to $x = 0$. We recalculate the value $N_{\max}$

$$K - \exp(x_{N_{\max}}) = 0 \rightarrow -\frac{x_{\max}}{2} + \delta_x N_{\max} = \log(K), \tag{36}$$

thus

$$N_{\max} = \left\lfloor (N_x - 1)\left(\frac{\log(K)}{2x_{\max}} + \frac{1}{4}\right)\right\rfloor. \tag{37}$$

Therefore, except normalization of the wave function, the coefficient of the eigenstate $\left|x_j\right\rangle$ is

$$K - \exp(-x_{\max}/2 + \delta_x j),$$

for $j = 0....N_{\max}$. Considering that due to the duplication each coefficient is repeated twice, the norm squared results to be

$$\Lambda = \left(2\sum_{m=0}^{N_{\max}}(K - \exp(-x_{\max}/2 + \delta_x m))^2\right).$$

Finally the normalized wave function is

$$\left|V_p\right\rangle = \sum_{i=0}^{N_{\max}} \frac{K - e^{-x_{\max}/2+\delta_x j}}{\Lambda^{1/2}}\left(\left|x_j\right\rangle + \left|x_{N_x-1-j}\right\rangle\right) = \sum_{i=0}^{N_x-1} c_j(K)\left|x_j\right\rangle. \tag{38}$$

We can use the work of Ref [52] to efficiently load Eq. 38 into a quantum computer.

C. Hamiltonian Change of Basis and Walsh Functions

In this section we present how to express our Hamiltonian in terms of Cartan basis. Suppose that we have a Hamiltonian expressed in terms of the canonical (projector) basis

$$H = \sum_{k=0}^{N_x-1} h_k \left|k\right\rangle\left\langle k\right|. \tag{39}$$

We calculate the coefficient of the projector $\left|k\right\rangle\left\langle k\right|$ in the $\sigma_0^{i_0}...\sigma_{n-1}^{i_{n-1}}$ element of the Cartan basis as

$$\frac{1}{N_x}\mathrm{tr}\left(\left|k\right\rangle\left\langle k\right|\sigma_0^{i_0}...\sigma_{n-1}^{i_{n-1}}\right) = \frac{1}{N_x}\left\langle k\right|\sigma_0^{i_0}...\sigma_{n-1}^{i_{n-1}}\left|k\right\rangle$$

$$= \frac{1}{N_x}\left\langle x_0...x_{n-1}\right|\sigma_0^{i_0}...\sigma_{n-1}^{i_{n-1}}\left|x_0...x_{n-1}\right\rangle = \frac{1}{N_x}(-1)^{\sum_{j=0}^{n-1} x_j i_j}, \tag{40}$$

where $k = \sum_{j=0}^{n-1} x_j 2^{n-1-j}$ and we define $x = \frac{k}{N_x} = \sum_{j=0}^{n-1} x_j 2^{-1-j}$ as the fraction with the same binary representation. Now we present Walsh Functions in order to understand the change of basis from canonical projector basis to Cartan basis. We define the family of Walsh Functions as:

$$W_I : [0,1] \rightarrow \{-1,1\}. \tag{41}$$

Given any natural number I, and real number $x \in [0,1]$, we define the I_{th} Walsh Function as

$$W_I(x) = (-1)^{\sum_{k=0}^{\infty} x_k i_k}, \tag{42}$$

where i_j is the j_{th} bit in the binary representation of I, starting with i_0 as the least significant bit, and x_j is the j_{th} bit in the binary representation of x, starting with x_0 as the most significant fractional bit. Considering this definition we can therefore express the coefficient of the projector $\left|k\right\rangle\left\langle k\right|$ in the $\sigma_0^{i_0}...\sigma_{n-1}^{i_{n-1}}$ element of the Cartan basis as

$$\frac{1}{N_x}W_I(x) \text{ where } I = \sum_{j=0}^{n-1} i_j 2^j \text{ and } x = \sum_{j=0}^{n-1} x_j 2^{-1-j}, \tag{43}$$

hence

$$\left|k\right\rangle\left\langle k\right| = \frac{1}{N_x}\sum_I W_I(x)\,\sigma_0^{i_0}...\sigma_{n-1}^{i_{n-1}}. \tag{44}$$

D. Hamiltonian coefficients

In the previous section of the appendix we showed which are the coefficients of the Hamiltonian expressed in the Cartan basis, Eq. (20). Now we present how to chose the most significative of them. We discuss two cases: the Hermitan Hamiltonian $\hat{H}_{\mathrm{BSH}}$ and the embedded Hamiltonian $\tilde{H}$.

In the Hermitian case, every non-zero term has to include the interaction $\hat{\sigma}_0^z$ and the interactions with an odd number of body interactions suppose the largest terms in general. For each non-zero term, Eq. (20) sums up to an analytical expression. We split the expressions into three categories: only first qubit interaction, interactions with an odd number of bodies, and interactions with an even number of bodies. Denoting by $0 = j_0 < j_1 < ... < j_{2k} \leq n-1$ the indices of the qubits on which the operators act, the reindexed coefficients $h'_{\boldsymbol{J}}$ of Eq. (20) are

$\underline{\hat{\sigma}_0^z\,\mathbb{I}_1 \ldots\, \mathbb{I}_{n-1}}$:

$$\frac{2^n-1}{2^{n+1}}\frac{2r-\sigma^2}{x_{\max}}\cot\left(\frac{\pi}{2^n}\right). \tag{45}$$

$\underline{\hat{\sigma}_{j_0=0}^z\hat{\sigma}_{j_1}^z ...\, \hat{\sigma}_{j_{2k}}^z}$:

$$(-1)^k\,\frac{2^n-1}{2^{n+1}}\frac{2r-\sigma^2}{x_{\max}}\cot\left(\frac{\pi}{2^n}\right)\tan\left(\frac{\pi}{2^{j_1+1}}\right)...\,\tan\left(\frac{\pi}{2^{j_{2k}+1}}\right). \tag{46}$$

$\underline{\hat{\sigma}_{j_0=0}^z\hat{\sigma}_{j_1}^z ...\, \hat{\sigma}_{j_{2k-1}}^z}$:

$$(-1)^k\,\frac{2^n-1}{2^{n+1}}\frac{2r-\sigma^2}{x_{\max}}\tan\left(\frac{\pi}{2^{j_1+1}}\right)...\,\tan\left(\frac{\pi}{2^{j_{2k-1}+1}}\right). \tag{47}$$

In the embedded case, the number of the interactions that play a relevant role, as seen in Fig 7, is minor, and every non-zero term has to discard the interaction $\hat{\sigma}_0^z$. Therefore we provide an approximation for the largest terms: $\mathbb{I}_0 \dots \mathbb{I}_{n-1}$ and $\mathbb{I}_0\hat{\sigma}_1^z\hat{\sigma}_2^z\mathbb{I}_3 \dots \mathbb{I}_{n-1}$.

$\underline{\mathbb{I}_0 \dots \mathbb{I}_{n-1}}$:

$$\frac{\pi}{2} - \frac{1}{2^n}\sum_{k=0}^{2^{n-1}}\left[\exp\left(-T\left(\frac{\sigma^2}{2}\frac{\sin^2(2\pi k/2^n)}{\delta_x^2} + r\right)\right)\right] \tag{48}$$

This is a good approximation from $n \geq 7$, and from $n \geq 10$ its value can be taken as the constant $\frac{\pi}{2}$, as the second term converges exponentially to 0 when $n \to \infty$, .

$\underline{\mathbb{I}_0\hat{\sigma}_1^z\hat{\sigma}_2^z\mathbb{I}_3 \dots \mathbb{I}_{n-1}}$:

In this case, for $n \geq 8$ the coefficient can be approximated by

$$\frac{1}{2^n}\left(2\arccos\left(\exp(-Tr)\right) - \pi\right)$$

$$+4\int_0^{\frac{1}{8}} \arccos\left(\exp\left(-T\left(\frac{\sigma^2}{2}\left(\frac{2^n-1}{2x_{max}}\right)^2\sin(2\pi x)^2 + r\right)\right)\right)dx$$

$$-4\int_{\frac{1}{8}}^{\frac{1}{4}} \arccos\left(\exp\left(-T\left(\frac{\sigma^2}{2}\left(\frac{2^n-1}{2x_{max}}\right)^2\sin(2\pi x)^2 + r\right)\right)\right)dx. \tag{49}$$

This term presents a decay factor $\frac{1}{2^n}$.

E. Index Degeneration

In this section we analyze the degeneration, $g_{I'}$ of the index $I' = \sum_{l=1}^{2k}(j_l - 1)$ with $0 = j_0 < j_1 < j_{2k} \leq n-1$, section V D. The problem is equivalent to solve the number of subsets of $X = \{0, \dots n-2\}$ of an even number of elements for which the sum of the members is I'. As proposed in [54], the number of partitions of a positive integer I' into distinct parts, each $\leq n-2$ is upper bounded by

$$g_{I'} < \left(\frac{2}{n^2-3n+4-4I'} + \frac{\pi}{2\sqrt{3I'}}\right)e^{(\pi/\sqrt{3} - \frac{e^{-\pi\left\lceil\frac{n-2}{2}\right\rceil\sqrt{3}}}{\pi\sqrt{3I'}})\sqrt{I'}}$$

$$\leq \left(\frac{2}{n^2-3n+4} + \frac{\pi}{2\sqrt{3}}\right)e^{(\pi/\sqrt{3})\sqrt{I'}} \tag{50}$$

for $I' \leq \frac{n}{4}(n-1)$. Considering that this degeneration distribution is symmetric with respect to the middle, where it reaches the maximum value, we can conclude that

$$g_{I'} < 2\left(\frac{2}{n^2-3n+4} + \frac{\pi}{2\sqrt{3}}\right)e^{(\pi/\sqrt{3})\sqrt{\frac{n}{4}(n-1)}} \tag{51}$$

where the factor 2 comes from the inclusion of the interactions with an even number of bodies. In order to simplify the notation, we define

$$C' = 2\left(\frac{2}{n^2-3n+4} + \frac{\pi}{2\sqrt{3}}\right)e^{(\pi/\sqrt{3})\sqrt{\frac{n}{4}(n-1)}}C, \tag{52}$$

where $C = \frac{2^n-1}{2^{n+1}}\frac{2r-\sigma^2}{x_{\max}}\cot\left(\frac{\pi}{2^n}\right)$.

F. Truncation Error

In this section, we detail the calculations to obtain an upper bound for the truncation error. To define this error, we consider the propagator corresponding to the excluded terms and compare it with the identity operator, thus

$$\xi(M) = \left\| e^{iT\sum_{I'=M}^{\frac{n}{2}(n-1)-1}\sum_{J|I'(J)=I'}h'_J\hat{c}_J} - e^{i\theta}\mathbb{I}\right\|_\infty = \max_j|\lambda_j| \tag{53}$$

where λ_j is the jth eigenvalue of $e^{iT\sum_{I'=M}^{\frac{n}{2}(n-1)-1}\sum_{J|I'(J)=I'}h'_J\hat{c}_J} - e^{i\theta}\mathbb{I}$.

Now, we proceed to upper bound the eigenvalues $|\lambda_j| = |\beta_j - e^{i\theta}| \quad \forall j$, where β_j is the jth eigenvalue of $e^{iT\sum_{I'=M}^{\frac{n}{2}(n-1)-1}\sum_{J|I'(J)=I'}h'_J\hat{c}_J}$. In the worst case scenario, the maximum rotation angle between two eigenstates β_j and $\beta_{j'}$, is $2\sum_{I'=M}^{\frac{n}{2}(n-1)-1}\sum_{J|I'(J)=I'}|h'_j| \leq 2C\sum_{I'=M}^{\frac{n}{2}(n-1)-1}\frac{g_{I'}}{2^{I'}} < 2\frac{2C'}{2^M}$, with C' a new constant depending on n and the financial parameters (see Appendix VII E). Taking M sufficiently large to guarantee that $C'/2^M \leq \pi/4$, this angle difference is less than π and evenly distributed around the real axis, hence the optimal gauge choice is $\theta = 0$. Thus, we can conclude that $\xi(M) = \max_j|\lambda_j| \leq |e^{iT\frac{2C'}{2^M}} - 1| = \sqrt{2\left(1-\cos(2TC'/2^M)\right)} = C(M)$, and therefore it is straighforward to obtain Eq. (26) .

If an error ϵ is allowed in our algorithm, we want to find the minimum number of terms, M_ϵ^ξ, needed to guarantee that the truncation error $\xi(M_\epsilon^\xi) < \epsilon \; \forall M > M_\epsilon^\xi$. As the expression $C(M) = \sqrt{2\left(1-\cos(2TC'/2^M)\right)} \underset{M\to\infty}{\longrightarrow} 0$ monotonically, we can define $M_\epsilon^C = \max\{M|C(M) \geq \epsilon\}$. Thus,

$$\epsilon \leq \sqrt{2\left(1-\cos\left(2TC'/2^{M_\epsilon^C}\right)\right)}, \tag{54}$$

$$\cos\left(2TC'2^{-M_\epsilon^C}\right) \leq 1 - \frac{\epsilon^2}{2}, \tag{55}$$

due to $\arccos(x)$ it is a decreasing function in $[\frac{1}{2}, 1]$

$$\arccos\left(1-\frac{\epsilon^2}{2}\right) \leq 2TC'2^{-M_\epsilon^C}, \tag{56}$$

and then

$$M_\epsilon^C \leq \log_2\left[\frac{1}{2TC'}\arccos\left(1-\frac{\epsilon^2}{2}\right)\right]^{-1}$$

$$= \log_2(2TC') - \log_2(\arccos(1-\epsilon^2/2)). \quad (57)$$

As $C(M)$ is an upper bound for the truncation error, $\xi(M)$, we have that $M_\epsilon^\xi \leq M_\epsilon^C$, and consequently $M_\epsilon^\xi \leq \log_2(2TC') - \log_2(\arccos(1-\epsilon^2/2))$.

G. Hamiltonian Implementation Circuit Details

In this section we show the quantum circuit corresponding to the truncated Black-Scholes Hamiltonian dynamics by using the circuit implementation proposed in Fig. 5 for operators of the form Eq. (21). We make use of 8+2 qubits and consider largest 14 Hermitian + 6 embedded interactions. We omit the already explained blocks of the circuit performing initialization, Quantum Fourier Transform and measurement.

In order to implement the non-Hermitian Hamiltonian dynamics we use an extra set of gates {Z,S,H}. First, in order to produce the embedding we need to use the $\hat{\sigma}^z$=Z=$\begin{pmatrix}1 & 0\\ 0 & -1\end{pmatrix}$ gate acting on q_E as we can see in Eq. (6). Then, we make use of the property Y=SHZHS†, where S=$\begin{pmatrix}1 & 0\\ 0 & i\end{pmatrix}$, H=$\frac{1}{\sqrt{2}}\begin{pmatrix}1 & 1\\ 1 & -1\end{pmatrix}$, $\hat{\sigma}^y$=Y=$\begin{pmatrix}0 & -i\\ i & 0\end{pmatrix}$, to express $e^{i\beta\,\hat{\sigma}^y_E\otimes(\hat{\sigma}^z_{i_1}\ldots.\,\hat{\sigma}^z_{i_k})}$ as $S^\dagger H e^{i\beta\,\hat{\sigma}^z_E\otimes(\hat{\sigma}^z_{i_1}\ldots.\,\hat{\sigma}^z_{i_k})}HS$ for every term in the exponential of the non-Hermitian Hamiltonian. Finally, for both Hamiltonians, we implement every exponential $e^{i\beta\,\hat{\sigma}^z_E\otimes(\hat{\sigma}^z_{i_1}\ldots.\,\hat{\sigma}^z_{i_k})}$ term as a β phase rotation whose sign depends on the parity of the state that is computed by using controlled NOT gates. There exist several alternatives to compute the parity of a state, in particular we choose to add an ancillary qubit q_G that tracks this property. This choice leads to the cancelation of some controlled NOT gates if we choose a proper order for the terms to be implemented. Each one of the boxed labeled operators acting on ancillary qubit q_G, consists in a phase rotation towards the z-axis, and the value of the angle rotation is given by the coefficient of the corresponding boxed vector. $C_{\hat{H}}$ denotes the Cartan vectors representation of the Hermitian Hamiltonian and $C_{\tilde{H}}$ the Cartan basis of the embedded decomposition.

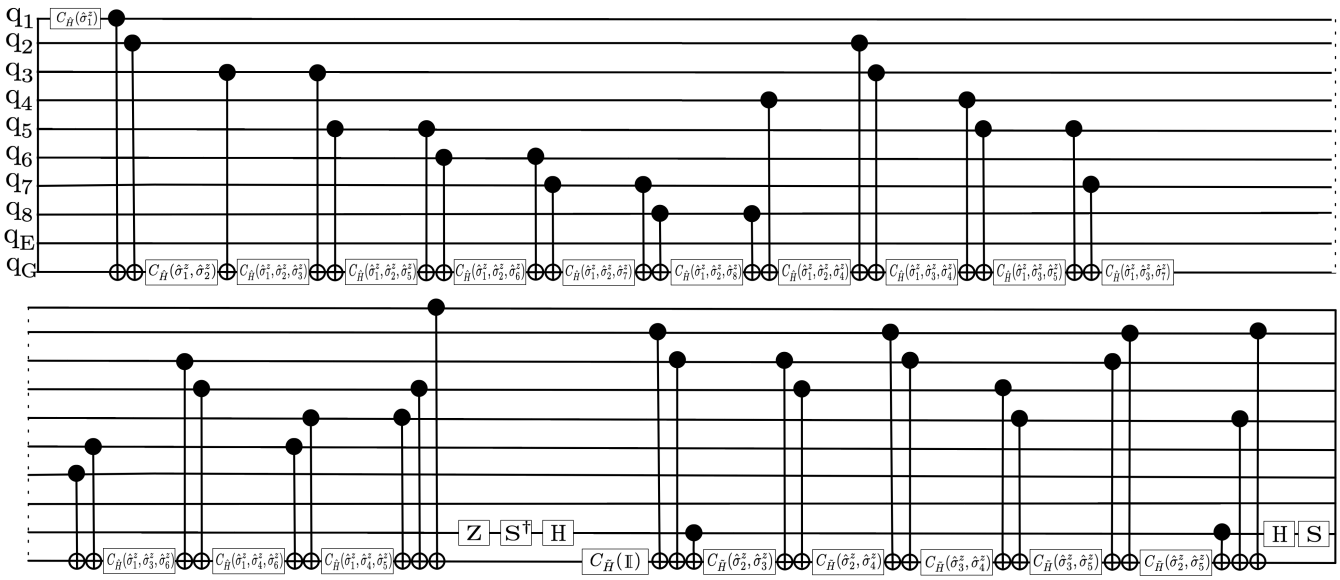

FIG. 10. Circuit gates implementation of Hermitian Hamiltonian and embedded dynamics proposed with 8 qubit and the 14+6 largest body interactions. Each one of the boxed labeled operators acting on ancillary qubit q_G, consists in a phase rotation towards the z-axis, and the value of the angle rotation is given by the coefficient of the corresponding boxed vector. $C_{\hat{H}}$ denotes the Cartan vectors of the Hermitian Hamiltonian and $C_{\tilde{H}}$ the basis of the embedded decomposition.

H. Success Probability

In this section we analyze the probability of recovering the desired dynamics given by the expression

$$
\begin{aligned}
Ps &= \left\langle V_p \right| \hat{O}^2(-t) \left| V_p \right\rangle = \left\langle V_p \right| \hat{F}^\dagger e^{-2T(\frac{\sigma^2}{2}\hat{P}_k^2 + r\mathbb{I})} \hat{F} \left| V_p \right\rangle \\
&= \frac{1}{N_x \Lambda} \sum_{k=0}^{N_x-1} \Bigg[\Bigg(\sum_{j=0}^{N_{\max}} (K - e^{-x_{\max}/2 + j\delta_x}) e^{2\pi i k j / N_x} + \\
&\quad \sum_{j=N-1-N_x}^{N_x-1} (K - e^{-x_{\max}/2 + (N_x-1-j)\delta_x}) e^{2\pi i k j / N_x} \Bigg) \\
&\quad \Bigg(\sum_{j'=0}^{N_{\max}} (K - e^{-x_{\max}/2 + j'\delta_x}) e^{-2\pi i k j'/N_x} + \\
&\quad \sum_{j'=N-1-N_x}^{N_x-1} (K - e^{-x_{\max}/2 + (N_x-1-j')\delta_x}) e^{-2\pi i k j/N_x} \Bigg) e^{-2T(\frac{\sigma^2}{2}\hat{P}_k^2 + r)} \Bigg]
\end{aligned}
\tag{58}
$$

where p_k is given by Eq. (12). Considering that all the terms are positive of the sum, the largest term corresponds to $k = 0$. Then considering only this term, the success probability can be lower bounded by the expression

$$
\begin{aligned}
P_s \geq \frac{1}{N_x \Lambda} e^{-2Tr} \Bigg[& \sum_{j,j'=0}^{N_{\max}} (K - e^{-\delta_x N_x/4 + j\delta_x})(K - e^{-\delta_x N_x/4 + j'\delta_x}) + \\
& \sum_{j,j'=N-1-N_x}^{N_x-1} (K - e^{-\delta_x N_x/4 + (N_x-1-j)\delta_x})(K - e^{-\delta_x N_x/4 + (N_x-1-j')\delta_x}) \\
& \sum_{j=0,j'=N-1-N_x}^{N_{\max},N_x-1} (K - e^{-\delta_x N_x/4 + j\delta_x})(K - e^{-\delta_x N_x/4 + (N_x-1-j')\delta_x}) + \\
& \sum_{j=N-1-N_x,j'=0}^{N_x-1,N_{\max}} (K - e^{-\delta_x N_x/4 + (N_x-1-j)\delta_x})(K - e^{-\delta_x N_x/4 + j'\delta_x}) \Bigg]
\end{aligned}
\tag{59}
$$

The four terms of this expression sum up to the same, then we define

$$
\begin{aligned}
\gamma_0(N_x, K) &= \sum_{j,j'=0}^{N_{\max}} (K - e^{-x_{\max}/2 + j\delta_x})(K - e^{-x_{\max}/2 + j'\delta_x}) \\
&= \frac{e^{-\delta_x N_x/2} \left(1 - e^{\delta_x (1+N_x)} + e^{\delta_x N_x/4} (-1 + e^{\delta_x} K (1 + N_{\max}) \right)^2}{(-1 + e^{\delta_x})^2}
\end{aligned}
\tag{60}
$$

and finally

$$
\gamma(N_x, K) = \frac{4\gamma_0}{\Lambda N}.
$$

I. Comparison to classical methods for solving PDEs

As a part of our study, we have also analyzed the performance of our quantum algorithm compared to classical techniques usually employed to solve Black Scholes PDE. In this context, Crank-Nicolson arises as the standard finite difference method [58] used for numerically solving the heat equation. In contrast to our algorithm, this method discretizes time, it is second-order method in time, what indeed supposes an extra limitation in the accuracy of the solution. Relative error of quantum algorithm and Crank-Nicolson solutions with respect to analytical are shown in Fig. 11. As we can observe, there is an asymptotic constant behaviour in Crank-Nicolson associated with the limitation introduced by time discretization.

Algorithm	Complexity
Quantum Simulation	$O(\text{poly}(n))$
Finite differences (explicit)	$O(T_{\text{steps}} 2^n)$
Finite differences (Crank-Nicolson)	$O(T_{\text{steps}} 2^n)$
Fast Fourier transform	$O((n+1)2^n)$
Matrix exponentiation	$O(2^n)$

TABLE II. Algorithms and their costs [43]. We compare the costs of different tasks when working with multivariate functions, from the construction of the state, to the simulation of their evolution. ϵ, desired error bound; N, number of variables; n number of qubits per variable for points in discretization T_{steps} is the number of time steps

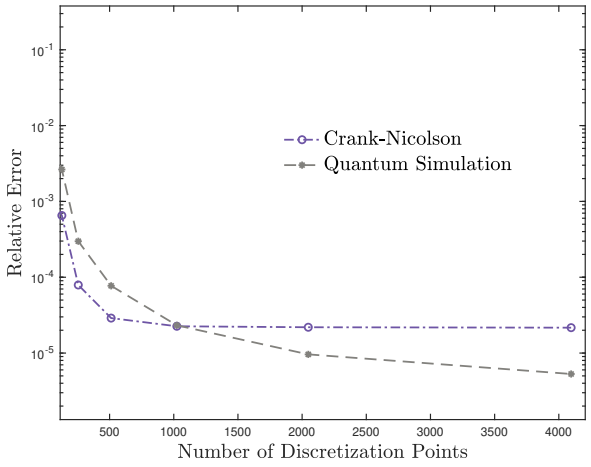

FIG. 11. Comparison of the accuracy, computed with the L^1-norm, reached for Crank-Nicolson scheme and the quantum algorithm. Crank-Nicolson shows better results when the number of discretization points is low, but time discretization effects limit this method when the grid has over 1000 points and we can appreciate how this technique gets stuck. In the opposite side, quantum algorithm improves its accuracy continuously as we enlarge the grid size.

We also provide in Table. II the comparison with other classical methods for solving partial differential equations, like the fast Fourier transform or matrix exponentiation techniques

[1] F. Black and M. Scholes, *The Pricing of Options and Corporate Liabilities*. The Journal of Political Economy **81**, 637 (1973).

[2] R.Valkov, *Fitted Finite Volume Method for a Generalized Black-Scholes Equation Transformed on Finite Interval*. ArXiv:1211.1903 (2012).

[3] J. A. Acebron, *A Monte Carlo method for computing the action of a matrix exponential on a vector*. ArXiv:1904.12759 (2019).

[4] W. C. Chen and W. H. Chung, *Option Pricing via Multi-path Autoregressive Monte Carlo Approach*. 61st Meeting of EURO Working Group for Commodities and Financial Modeling, 16-18 MAY 2018, Kaunas, Lithuania.

[5] G. Krzyżanowski, M. Magdziarz, and Ł. Płociniczak, *A weighted finite difference method for subdiffusive Black Scholes Model*. ArXiv:1907.00297 (2019).

[6] G. Krzyżanowski and M. Magdziarz, *A computational weighted finite difference method for American and barrier options in subdiffusive Black-Scholes model*. ArXiv:2003.05358 (2020).

[7] F. Arute, K. Arya, R. Babbush *et al*, *Quantum supremacy using a programmable superconducting processor*. Nature **574**, 505 (2019).

[8] D. J. Egger, C. Gambella, J. Marecek, S. McFaddin, M. Mevissen, R. Raymond, A. Simonetto, S. Woerner, and E. Yndurain, *Quantum computing for Finance: state of the art and future prospects*. IEEE Transactions on Quantum Engineering (2020).

[9] R. Orús, S. Mugel, and E. Lizaso, *Quantum computing for finance: Overview and prospects*. Reviews in Physics **4**, 100028 (2019).

[10] R. Orús, S. Mugel, and E. Lizaso, *Forecasting financial crashes with quantum computing*. Phys. Rev. A **99**, 060301(R) (2019).

[11] Y. Ding, J. Gonzalez-Conde, L. Lamata, J. D. Martín-Guerrero, E. Lizaso, S. Mugel, X. Chen, R. Orús, E. Solano, and M. Sanz, *Towards Prediction of Financial Crashes with a D-Wave Quantum Computer*. ArXiv:1904.05808 (2019).

[12] A. Martin, B. Candelas, A. Rodríguez-Rozas, J. D. Martín-Guerrero, X. Chen, L. Lamata, R. Orús, E. Solano, and M. Sanz, *Towards Pricing Financial Derivatives with an IBM Quantum Computer*. ArXiv:1904.05803 (2019).

[13] D. Venturelli and A. Kondratyev, *Reverse quantum annealing approach to portfolio optimization problems*. Quantum Mach. Intell. (2019)

[14] P. Rebentrost and S. Lloyd, *Quantum computational finance: quantum algorithm for portfolio optimization*. ArXiv:1811.03975 (2018).

[15] S. Mugel, C. Kuchkovsky, E. Sanchez, S. Fernandez-Lorenzo, J. Luis-Hita, E. Lizaso, and R. Orús, *Dynamic Portfolio Optimization with Real Datasets Using Quantum Processors and Quantum-Inspired Tensor Networks*. ArXiv:2007.00017 (2020).

[16] J. Cohen, A. Khan, and C. Alexander, *Portfolio Optimization of 40 Stocks Using the D-Wave Quantum Annealer*. ArXiv:2007.01430 (2020).

[17] J. Cohen, A. Khan, and C. Alexander, *Portfolio Optimization of 60 Stocks Using Classical and Quantum Algorithms*. ArXiv:2008.08669 (2020).

[18] B. Coyle, M. Henderson, J. C. J. Le, N. Kumar, M. Paini, and E. Kashefi, *Quantum versus Classical Generative Modelling in Finance*. ArXiv:2008.00691 (2020).

[19] H. Tang, A. Pal, L. F. Qiao, T. Y. Wang, J. Gao, and X. M. Jin, *Quantum Computation for Pricing the Collateral Debt Obligations*. ArXiv:2008.04110 (2020).

[20] L. Braine, D. J. Egger, J. Glick, and S. Woerner, *Quantum Algorithms for Mixed Binary Optimization applied to Transaction Settlement*. ArXiv:1910.05788 (2019).

[21] S. Woerner and D. J. Egger, *Quantum risk analysis*. Npj Quantum Inf **5**, 15 (2019).

[22] D. J. Egger, R. G.Gutiérrez, J. C. Mestre, S. Woerner, *Credit Risk Analysis using Quantum Computers*. ArXiv:1907.03044 (2019).

[23] P. Rebentrost, B. Gupt, and T. R. Bromley, *Quantum computational finance: Monte Carlo pricing of financial derivatives*. Phys. Rev. A **98**, 022321 (2018).

[24] N. Stamatopoulos, D. J. Egger, Y. Sun, C. Zoufal, R. Iten, N. Shen, and S. Woerner, *Option Pricing using Quantum Computers*. Quantum **4**, 291 (2020).

[25] D. Grinko, J. Gacon, C. Zoufal, and S. Woerner, *Iterative Quantum Amplitude Estimation*. ArXiv:1912.05559 (2019).

[26] S. Chakrabarti, R. Krishnakumar, G. Mazzola, N. Stamatopoulos, S. Woerner, and W. J. Zeng, *A Threshold for Quantum Advantage in Derivative Pricing*. ArXiv:2012.03819 (2020).

[27] S. Ramos-Calderer, A. Pérez-Salinas, D. García-Martín, C. Bravo-Prieto, J. Cortada, J. Planagumà, and J. I. Latorre, *Quantum unary approach to option pricing*. ArXiv:1912.01618 (2019).

[28] A. Montanaro and S. Pallister, *Quantum algorithms and the finite element method*. Phys. Rev. A **93**, 032324 (2016).

[29] A. M. Childs, J. Liu, and A. Ostrandertextit, *High-precision quantum algorithms for partial differential equations*. ArXiv:2002.07868 (2020).

[30] T. Xin, S. Wei, J. Cui, J. Xiao, I. Arrazola, L. Lamata, X. Kong, D. Lu, E. Solano, and G. Long, *Quantum algorithm for solving linear differential equations: Theory and experiment*. Phys. Rev. A **101** 032307 (2020).

[31] R. Di Candia, B. Mejia, H. Castillo, J. S. Pedernales, J. Casanova, and E. Solano, *Embedding Quantum Simulators for Quantum Computation of Entanglement*. Phys. Rev. Lett. **111**, 240502 (2013).

[32] D. W. Berry, G. Ahokas, R. Cleve, and B. C. Sanders, *Efficient quantum algorithms for simulating sparse Hamiltonians*. Comm. Math. Phys. **270**, 359 (2007).

[33] A. M. Childs, D. Maslov, Y. Nam, N. J. Ross, and Y. Su, *Toward the first quantum simulation with quantum speedup*. PNAS **115**, 9456 (2018).

[34] D. W. Berry, A. M. Childs, and R. Kothari, *Hamiltonian simulation with nearly optimal dependence on all parameters*. FOCS, pp. 792 (2015).

[35] P. C. S. Costa, S. Jordan, and A. Ostrander, *Quantum Algorithm for Simulating the Wave Equation*. Phys. Rev. A **99**, 012323 (2019).

[36] A. Suau, G. Staffelbach, and H. Calandra, *Practical Quantum Computing: solving the wave equation using a quantum approach*. ArXiv:2003.12458 (2020).

[37] L. Jin and Z. Song, *Physics counterpart of the PT non-Hermitian tight-binding chain*. Phys. Rev. A **81**, 032109 (2010).

[38] B. E. Baaquie, *Quantum Finance Hamiltonians and Path Integrals for Options* (Cambridge University Press, Cambridge, 2004).

[39] R. Wulf, *Lie Groups – An Introduction Through Linear Groups*. (Oxford Science Publications, 2002).

[40] T. Constantinescu, *Schur Parameters, Dilation and Factoriza-*

tion Problems. Vol **82**, (Birkhäuser Verlag, 1996),

[41] C. E. Shannon, *Communication in the presence of noise*. Proceedings of the Institute of Radio Engineers **37**, (1949).

[42] N. Klco and M. J. Savage, *Digitization of Scalar Fields for Quantum Computing*. Phys. Rev. A **99**, 052335 (2019).

[43] J. J. García-Ripoll, *Quantum-inspired algorithms for multivariate analysis: from interpolation to partial differential equation*. Quantum **5**, 431 (2021).

[44] M. A. Nielsen and I. L. Chuang, *Quantum Computation and Quantum Information* (Cambridge University Press, Cambridge, 2000).

[45] M. Plesch and Č. Brukner, *Quantum state preparation with universal gate decompositions.* Phys. Rev. A **83**, 032302 (2011).

[46] A. Macridin, P. Spentzouris, J. Amundson, and R. Harnik, *Digital quantum computation of fermion-boson systems*. Phys. Rev. A **98**, 042312 (2018).

[47] M. Möttönen, J. J. Vartiainen, V. Bergholm, and M. M. Salomaa, *Transformation of quantum states using uniformly controlled rotations*. Quant. Inf. Comp. **5**, 467 (2005)

[48] V.V. Shende, S. S. Bullock, and I. L. Markov, *Synthesis of Quantum Logic Circuits*. IEEE Trans. on Computer-Aided Design, vol. **25**, (2006)

[49] N.J. Ward, I. Kassal, and A. Aspuru-Guzik, *Preparation of many-body states for quantum simulation*. J. Chem. **Phys**. 130, 194105 (2009)

[50] A. C. Vazquez and S.Woerner, *Efficient State Preparation for Quantum Amplitude Estimation*. ArXiv:2005.07711 (2020).

[51] M. Schuld and F. Petruccione, *Supervised Learning with Quantum Computers*. OCLC: 1076208411 (2019).

[52] G. Marin-Sanchez, J. Gonzalez-Conde and M. Sanz, *Quantum algorithms for approximate function loading*. ArXiv:2111.07933 (2021).

[53] L. Hales and S. Hallgren, *Quantum Computation and Quantum Information* Proceedings of the 41st Annual Symposium on Foundations of Computer Science, 515 (2000).

[54] M. Bidar *Partition of an Integer into Distinct Bounded Parts,Identities and Bounds*. Integers, **12**, 445, (2012).

[55] A. Kipnis, A. J. Goldsmith, T. Weissman, Y. C. Eldar, *Distortion rate function of sub-Nyquist sampled Gaussian sources corrupted by noise*. 51st Annual Allerton Conference on Communication, Control, and Computing (2013).

[56] N. Ahmed and K.R. Rao , *Orthogonal Transforms for Digital Signal Processing*. (Springer Berlin Heidelberg 2012).

[57] A. Kipnis, Y. C. Eldar and A. J. Goldsmith, *Analog-to-Digital Compression: A New Paradigm for Converting Signals to Bits*. ArXiv:1801.06718 (2018).

[58] J. Crank and P. Nicolson, *A practical method for numerical evaluation of solutions of partial differential equations of the heat conduction type*. Proc. Camb. Phil. Soc. **43** (1947).